INTERNATIONAL JOURNAL FOR NUMERICAL AND ANALYTICAL METHODS IN GEOMECHANICS
*Int. J. Numer. Anal. Meth. Geomech.*, **23**, 1281–1307 (1999)

# COUPLED THERMO-HYDRO-MECHANICAL MODELLING OF BENTONITE BUFFER MATERIAL

T. KANNO,*[1] T. FUJITA[1], S. TAKEUCHI[1], H. ISHIKAWA[1], K. HARA[2] AND M. NAKANO[3]

[1] *Waste Technology Development Division, Power Reactor and Nuclear Fuel Development Corporation, Tokai Works, Tokai-mura, Ibaraki-ken 319-11, Japan*
[2] *Radioactive Waste Management Project, Power Reactor and Nuclear Fuel Development Corporation, 1-9-13 Akasaka, Minato-ku, Tokyo 107, Japan*
[3] *Faculty of Agriculture, University of Tokyo, 1-1-1 Yayoi, Bunkyo-ku, Tokyo 113, Japan*

## SUMMARY

Mechanistic model development and numerical analyses were carried out on coupled thermo-hydraulic-mechanical processes in bentonite-based buffer material for the geological disposal of high-level radioactive waste with small-scale laboratory experiments and a full-scale test. The mechanism of water movement in compacted bentonite was identified by applying theoretical equations to the experimental results. The application clearly explained the observed results of the temperature dependence of the hydraulic conductivity in the saturated state and the water diffusivity in the unsaturated state for the compacted bentonite and the dry density dependence of the diffusivity. The full-scale coupled test, BIG-BEN, was conducted at PNC (Power Reactor and Nuclear Fuel Development Corporation) Tokai Works. The results of the numerical analyses for the full-scale test which are based on the present knowledge of coupled processes and our small-scale experiments were in good agreement with the measured results except for mechanical phenomena. Copyright © 1999 John Wiley & Sons, Ltd.

KEY WORDS: bentonite; radioactive waste disposal; coupled analysis; hydraulic conductivity; water diffusivity; swelling pressure

## INTRODUCTION

Geological disposal of High-Level Radioactive Waste (HLW) in Japan in based on a multibarrier system composed of engineered and natural barriers.[1] The engineered barriers are composed of vitrified waste confined within a canister, overpack and buffer material. Benotonite clay, in a highly compacted from, is considered to be one of the most promising candidate buffer material mainly because of its low hydraulic conductivity and high adsorption capacity of radionuclides. In a repository for HLW waste, complex Thermo-Hydro-Mechanical (T-H-M) phenomena involving interactive processes such as the decay heat of vitrified waste, the infiltration of groundwater and the stress generation due to the ground pressure, the thermal loading and swelling pressure of the buffer material will take place. In order to evaluate the performance of the buffer material, the coupled T-H-M processes within the compacted bentonite need to be

* Correspondence to: Mr. Takeshi Kanno, Nuclear Fuel Cycle Development Department, Nuclear Power Division, Ishikawajima-Harima Heavy Industries Co., Ltd. Yokohama Engineering Center 1, Shin-nakahara-cho, Isogo-ku, Yokohama 235-8501 Japan. E-mail: takeshi_kanno@ihi.co.jp

CCC 0363–9061/99/121281–27$17.50

*Received September 1996*
*Revised 14 December 1998*

modelled. Before establishing a fully coupled T-H-M model, each single phenomenon or partially coupled phenomena should be identified and modelled physically and numerically. In this study, the temperature dependence of premeability in the saturated state and two-phase flow under isothermal condition are investigated as well as the analysis of a full-scale coupled T-H-M test.

The primary function of the buffer material is to retard groundwater movement through its low permeability. The temperature dependence of the permeability is important to understand because the temperature of the buffer material will increase due to the decay heat of the waste and the thermal condition deep underground. The permeability of bentonite buffer has usually been evaluated as the hydraulic conductivity by applying Darcy's law.[1–4] Radhakrishna and Chan[3] suggested that the effects of high temperature on the hydraulic conductivity of compacted clays are primarily attributed to the change in viscosity of the pore water and the permeant. However, quantitative evaluation of temperature effects on the hydraulic conductivity of bentonite-based buffer material has not been presented yet. If the change in the viscosity of pore water is the predominant reason for the temperature dependence of the hydraulic conductivity, the dependence can be explained by the intrinsic permeability concept.[5] This study evaluates the temperature dependence of the hydraulic conductivity of compacted bentonite applying the concept.

Under unsaturated conditions, water movement within the buffer material has often been expressed as a simple diffusion model with a constant apparent water diffusivity.[1,6,7] However, the above simple model is rather phenomenological and the dependence of diffusivity on water content has not been examined yet. Water movement in unsaturated porous media is known as a transfer process in both vapour and liquid phases.[8,9] Therefore, mathematical models should take the two-phase contribution into consideration. In this study, the water retention curves and water diffusivity of compacted bentonite are obtained as functions of water content, dry density and temperature. The water movement behaviour is examined by applying the Philip and de Vries[8] and Darcy's equations to the obtained water diffusivities.

Besides these mechanistic modelling with small-scale laboratory experiments, to develop a model of coupled T-H-M processes and to improve the construction technology of buffer material, a full-scale test facility for engineered barrier system (Big-Bentonite Facility: BIG-BEN), based on a pit disposal concept[1] was designed and constructed at Tokai Works, Power Reactor and Nuclear Fuel Development Corporation (PNC) in November, 1989. As the first stage of the BIG-BEN test, a heating experiment was carried out.[10] This paper also presents the results of a heating test with uniform water injection and numerical analyses for the test.

## THEORY OF WATER MOVEMENTS IN SATURATED/UNSATURATED STATE

### *Saturated state*

The hydraulic conductivity $k_{sat}$ of a saturated porous medium is determined from the volumetric flow rate $Q_{vol}$ and the hydraulic gradient $i$ according to the Darcy's law

$$Q_{vol} = k_{sat}\, Ai \tag{1}$$

where $A$ is the cross-sectional area. The intrinsic permeability[5] $\kappa$ of the medium is calculated from the hydraulic conductivity using

$$k_{sat} = \kappa \rho_l g / \mu \tag{2}$$

 

where $\rho_l$ is the density of liquid water, $\mu$ is the viscosity of water and $g$ is the gravitational constant. The intrinsic permeability depends solely on properties of the solid matrix such as grain size distribution, shape of grains, tortuosity, specific surface, and porosity.[5]

*Unsaturated state*

The one-dimensional water movement in a column of unsaturated bentonite is expressed by the following equation:[9]

$$Q = -k\frac{\partial \Psi}{\partial z} \tag{3}$$

where $Q$ is the flux of water, $k$ is unsaturated hydraulic conductivity which is a function of the degree of saturation and equal to $k_{\mathrm{sat}}$ at saturation, $z$ is the elevation and $\Psi$, the total potential of pore water in the bentonite, is composed of the matric potential, the gravity potential and the osmotic potential. Various definitions are given to the potentials: energy per unit mass (joules per kilogram), energy per unit volume (pascal), and energy per unit weight (meter).[11] In this study, the potentials are defined as energy per unit weight whose dimensions are identical to those of length or pressure head. The water potential $\Psi_w$, defined as the sum of the matric and osmotic potentials, is calculated from the relative humidity $P/P_0$ by the following equation:[8]

$$\Psi_{\mathrm{w}} = \frac{RT}{Mg}\ln\frac{P}{P_0} \tag{4}$$

where $M$ is the molecular weight of water, $R$ is the gas constant, $T$ is the absolute temperature, $P$ is the vapour pressure of sample and $P_0$ is the saturated vapour pressure.

Since the effects of the gravity and osmotic potentials are negligible in the case of bentonite,[12] the water flux is given by

$$Q = -k\frac{d\varphi}{\mathrm{d}\theta}\frac{\partial \theta}{\partial z} = -D\frac{\partial \theta}{\partial z} \tag{5}$$

in which

$$D = k\frac{\mathrm{d}\varphi}{\mathrm{d}\theta} \tag{6}$$

where $D$ is the water diffusivity, $\theta$ is the volumetric water content (VWC) and $\varphi$ is the matric potential. Then the water diffusivity is calculated by the following equation based on the distribution of VWC obtained by infiltration experiments:[12]

$$D = \frac{\displaystyle\int_{z_i}^{l} (\theta_{t=t_2} - \theta_{t=t_1})\ \mathrm{d}z}{1/2\ \{(\partial\theta/\partial z)_{z=z_i}^{t=t_2} + (\partial\theta/\partial z)_{z=z_i}^{t=t_1}\}} \times \frac{1}{t_2 - t_1} \tag{7}$$

where $t$ is infiltration time, $l$ is the length of the specimen and $z_i$ ($0 \leqslant z_i \leqslant l$) is the distance from the bottom of the specimen.

 

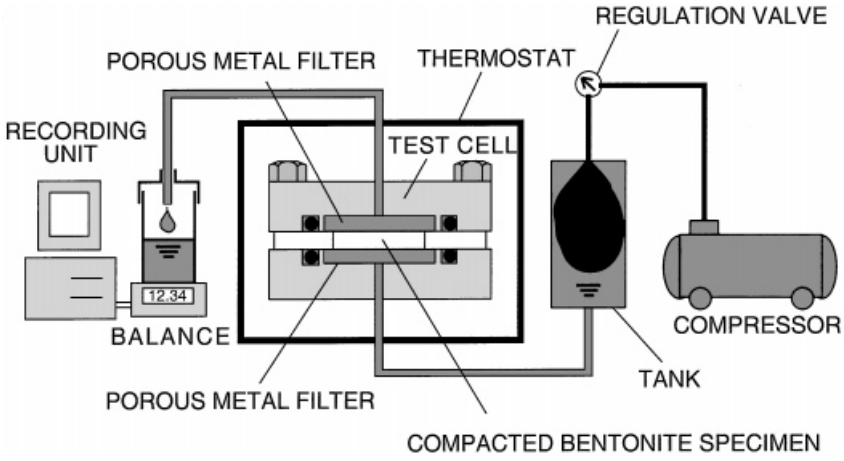


Figure 1. Schematic of test apparatus of hydraulic conductivity

## EXPERIMENTAL METHOD

As a reference sample, natural sodium bentonite[13] (Kunigel V1™, provided by Kunimine Industries Co., Ltd.) was used in this study.

### *Measurement of intrinsic permeability*

Two samples, pure bentonite (Kunigel V1) and a mixture of the Kungiel V1 (70 wt%)/quartz sand (30 wt%) were used. The samples were compacted uniaxially and statistically to dry densities of 1.4, 1.6 and 1.8 g/cm$^3$ in rigid stainless-steel cells, shown in Fig. 1, for constant-head permeability tests. The diameter of the cells was 50 mm and the thickness of the compacted specimens was 5 mm. Distilled water pressurized by compressed air was supplied into the cell, and the volumetric flow rate was determined by weighting the effluent as a function of time. The pressure of the compressed air was maintained at 0·8 MPa during the tests, that is the hydraulic gradient applied to the specimens was 16,000. In this study, the following heating–cooling procedure for each bentonite specimen with a thermostat was adopted taking into account the thermal condition of a repository:

$25 \rightarrow 40 \rightarrow 60 \rightarrow 80 \rightarrow 90 \rightarrow 80 \rightarrow 60 \rightarrow 40 \rightarrow 25^{\circ}C.$

### *Measurements of water potential and water diffusivity*

1. *Water potential.* The water potential of pure bentonite (Kunigel V1) specimens with various initial water contents was measured by a thermocouple psychrometer (Decagon Devices, Inc., SC10A) in a thermostat (Figure 2). The diameter of the specimens was 13 mm and the height was 9 mm. The psychrometer senses the relative humidity of vapour in equilibrium with the liquid phase in the bentonite. From the measured relative humidity, the water potential can be obtained

 

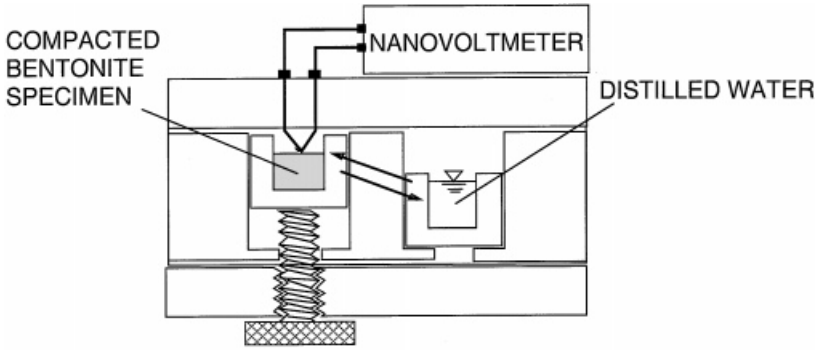


Figure 2. Schematic of thermocouple psychrometer

Table I. Test condition for the measurement of water potential

| Specimen | Kunigel V1 (Φ13 mm × 9H mm) | |
|---|---|---|
| Dry density | 1·6 (g/cm$^3$) | 1·8 (g/cm$^3$) |
| Temperature | 25°C | 25, 60°C |

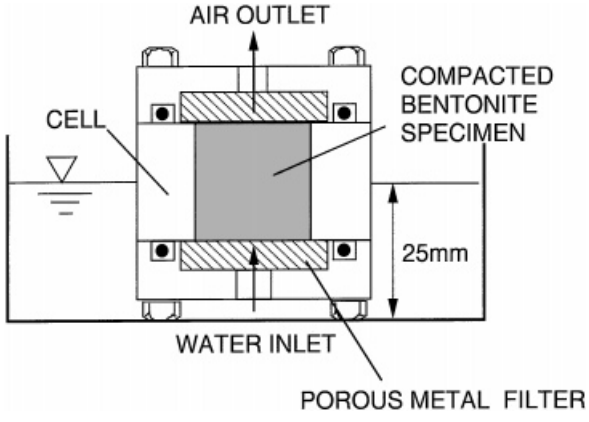


Figure 3. Schematic of test apparatus of water diffusivity

by equation (4). Since the matric potential is the dominant component of the water potential in the working range of the psychrometer,[11] the water potential obtained by the measurement is taken as the matrix potential ($\Psi_w = \varphi$). The VWC of the specimens were measured by an oven-drying method (110°C, 24 h). Then the water retention curve (WRC) was obtained by plotting the water potential as a function of VWC. The temperature and dry density for the experiment were 25, 60°C and 1.6, 1.8 g/cm$^3$ (Table I).

*2. Water diffusivity.* Water diffusivities were obtained by isothermal infiltration experiments. The compacted pure bentonite specimens (diameter 20 mm, height 20 mm) were set in stainless-steel cells (Figure 3) and water was supplied to the specimen from the bottom. The specimen was

 

Table II. Test condition for the measurement of water diffusivity

| Temperature (°C) | 25 | 40, 60 |
|---|---|---|
| Specimen | Kunigel V1 (Φ20 mm × 20H mm) | |
| Dry density (g/cm$^3$) | 1·0, 1·6, 1·8 | 1.8 |
| Duration time (h) | 4, 8, 16, 24, 48, 72 | |

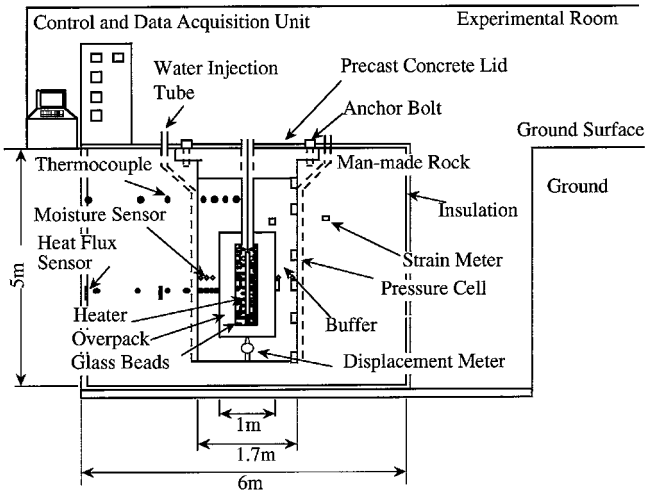


Figure 4. Schematic of BIG-BEN facility

sliced into 1 mm sections after various infiltration periods. The VWC of each section was measured by the over-drying method. The temperature and dry density of the experiment were in the ranges of 25–60°C and 1·0–1·8 g/cm$^3$ (Table II).

*The BIG-BEN test*

Figure 4 shows the schematic view of the BIG-BEN facility. The BIG-BEN experimental setup is composed of an electric heater, glass beads, a simulated overpack of carbon steel, buffer material and cylindrical man-made rock with a pit. The manmade rock, made of reinforced concrete, has a diameter of 6 m and a height of 5 m. The pit, approximately 1·7 m in diameter and 4·5 m in depth, is located in the centre of the man-made rock. The electric heater is set in the simulated overpack which is about 1 m in diameter and about 2 m in height.

A mixture of 70 wt% bentonite (Kunigel V1) and 30 wt% quartz sand was compacted by a tamper directly in the pit. The initial water content is 16·5% (volumetric water content is 26·4%) and the theoretical saturated water content is 26·5% percent (volumetric water content is 40·7%) by assuming no changes in the dry density and porosity. The annular space, 2 cm gap, between the simulated overpack and the buffer material was filled with quartz sand, and

 

Table III. Specification of sensors used in BIG-BEN test

| Measured item | Sensor | Number |
|---|---|---|
| Temperature | *K*-type sheathed thermocouples [JIS C 1602]: diameter 1·6 mm/heater, overpack, buffer diameter 3·2 mm/man-made rock | 139 |
| Heat flux | Heat flow meter:<br>Temp. range $-250$ to $+280$°C/overpack<br>Temp. range $-50$ to $+120$°C/man-made rock | 8 |
| Water content of buffer material | Gypsum moisture block: range 5–25%<br>Heat probe moisture: range 5–25% Humidity meter: range below 13% Psychrometer: range above 17% | 38 |
| Displacement of overpack | Strain gauge type displacement meter: Capacity 50 mm | 1 |
| Strain of man-made rock | Strain gauge: Capacity $\pm 1000 \times 10^{-6}$ | 12 |
| Swelling pressure of buffer material | Pressure cell:<br>max. 20 MPa | 20 |
| Stress of buffer material | Pressure cell: max. 5 MPa | 4 |
| Pore water pressure | Pressure cell: max. 5 MPa Pore water pressure meter: max. 2 MPa | 4 |
| Water pressure of water tube | Pressure meter: max. 5 MPa | 1 |

permeable mats packed with quartz sand were set in the space, 3 cm gap, between the buffer material and man-made rock. The heating-uniform water injection test was conducted with the operations of the heater and a water injection system. The heating simulates the decay heat of the waste and the water injection simulates groundwater seepage from the rock surrounding a disposal pit. The heater was operated at 0·8 kW to keep the temperature of buffer material below 100°C. The water was injected at the pressure of 0·05 MPa.

Sensors to monitors temperature, heat flux, water content, displacement of the overpack and swelling pressure were set in the buffer material and the man-made rock (Table III). Except for the swelling pressure, data acquisition was made hourly with a personal computer. Gypsum moisture block, heat probe, humidity meter, and psychrometer were used to monitor water content in the buffer material. To determine the water content distribution, the buffer material was sampled by a split-spoon sampler after 5 months and the water contents were measured by the oven-drying method. The swelling pressure was measured manually with pressure cells installed at the surface of the pit. The pressure cell consists of a 7 cm × 14 cm pad filled with mercury and equipped with a valve that opens when pressure is equal to or greater than that of the mercury.

## EXPERIMENTAL RESULTS

### *Measurement of intrinsic permeability*

The measured values of the hydraulic conductivities increased during the heating period and decreased during the cooling period for all specimens of both the pure and mixed samples as shown in Figure 5. No significant difference between measured hydraulic conductivities at the

 

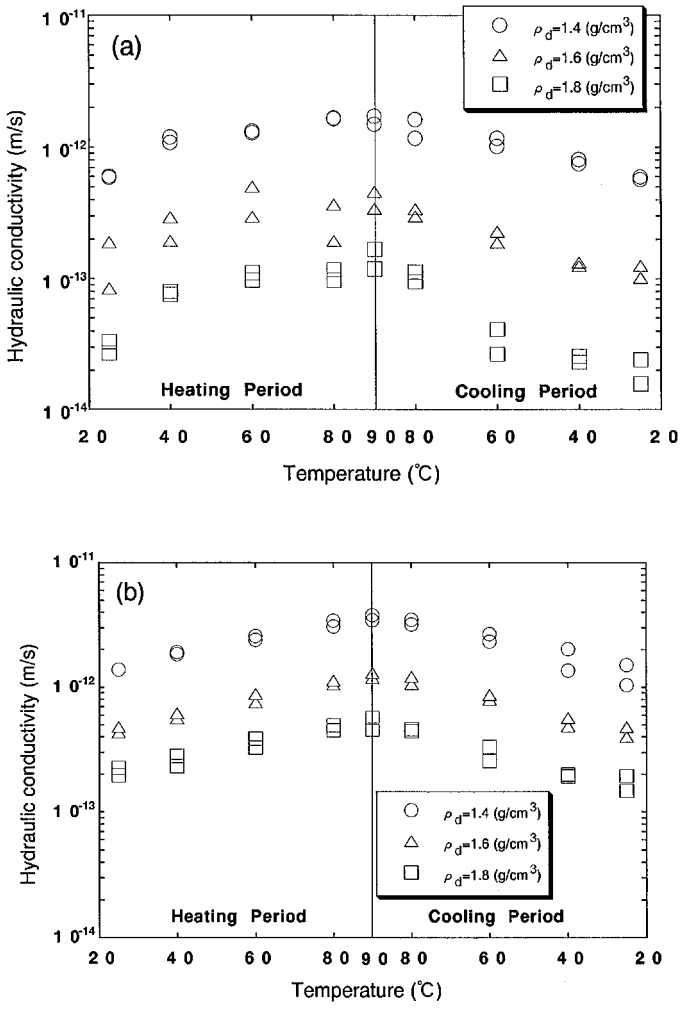


Figure 5. Measured results of hydraulic conductivities (a) Pure bentonite sample (b) Mixture sample

same temperature in heating and cooling periods is detected. The calculated results with equation (2) of the intrinsic permeability of the pure and mixed specimens are shown in Figure 6. The intrinsic permeability is independent of temperature.

*Measurements of water potential and water diffusivity*

*1. Water potential.* The WRCs determined from the psychrometric measurements are shown in Figures 7 and 8 in which the water potential is expressed as suction. The suction, negative pressure in the conventional notion, is converted into absolute value of water head in cm. The

 

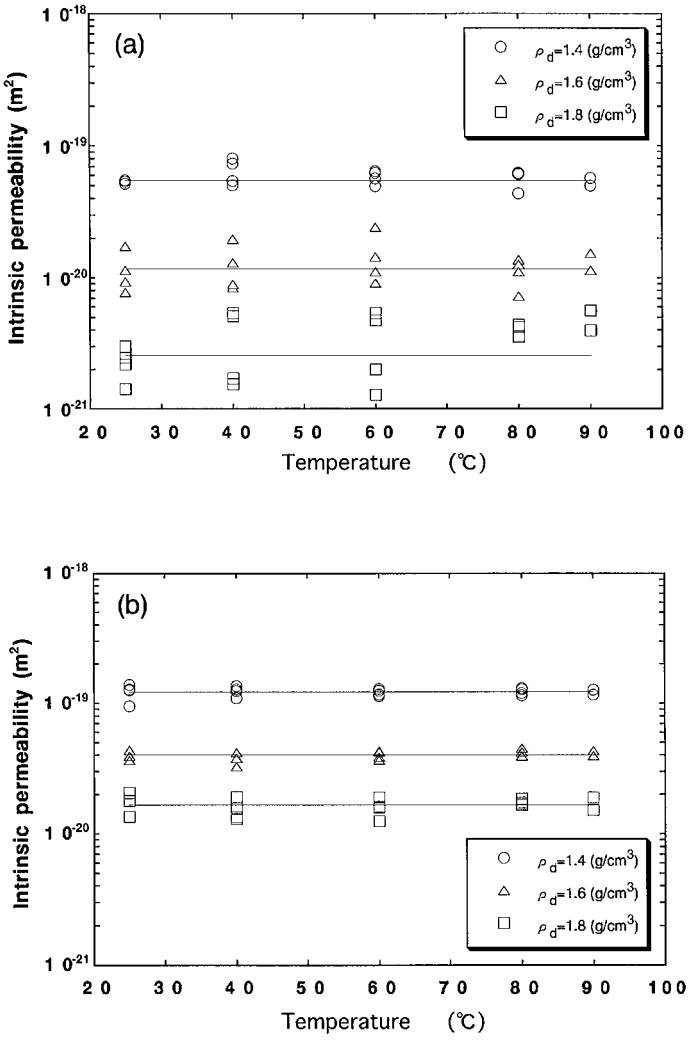


Figure 6. Temperature dependence of intrinsic permeability (a) Pure bentonite sample (b) Mixture sample

WRC fitted by the Van Genuchten's function,[14] depends on the dry density and temperature. The suction increases with dry density at lower VWC, however the suction seems to decrease with dry density at higher VWC. Also the suction decrease as temperature increases.

*2. Water diffusivity.* The distributions of the VWC obtained from the infiltration experiments for the specimens with the dry density of 1·6 g/cm$^3$ are shown in Figure 9. The distributions of the VWC of other conditions also show the same tendency as this case. Using equation (7), the water diffusivities calculated from the distributions of the VWC as the functions of the VWC at the ends of the infiltration experiments are shown in Figures 10 and 11. The water diffusivity depends on

 

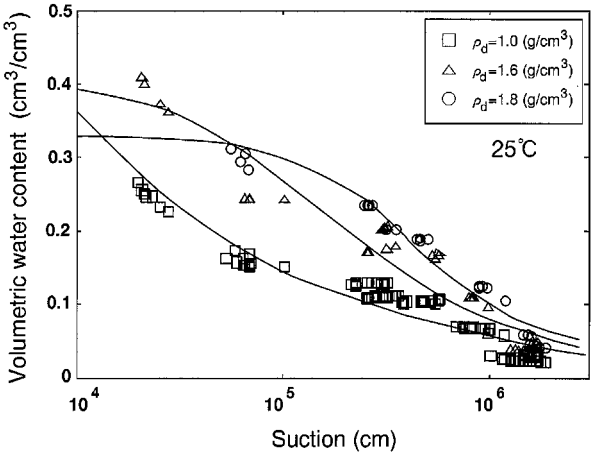


Figure 7. Dry density dependence of water retention curve

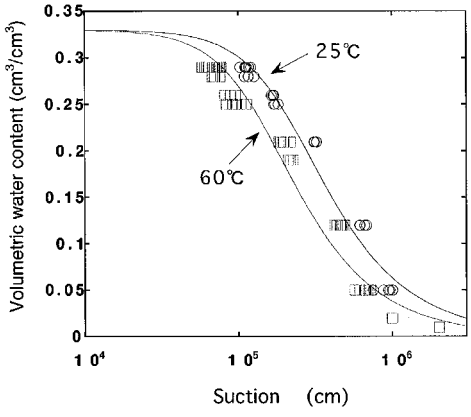


Figure 8. Temperature dependence of water retention curve

the VWC, and can be expressed as U-shaped curves. And the minimum value of the water diffusivity increases with the increases in the dry density and temperature.

In order to verify the measured results of the water diffusivity, the distributions of the VWC for each infiltration period were computed by a Finite Element Method (FEM) code named FINAS,[15] using the water diffusivities obtained as the function of the dry density and temperature from the experiments. The combination of equation (5) and the following continuity equation

$$\frac{\partial \theta}{\partial t} + \frac{\partial Q}{\partial z} = 0 \tag{8}$$

 

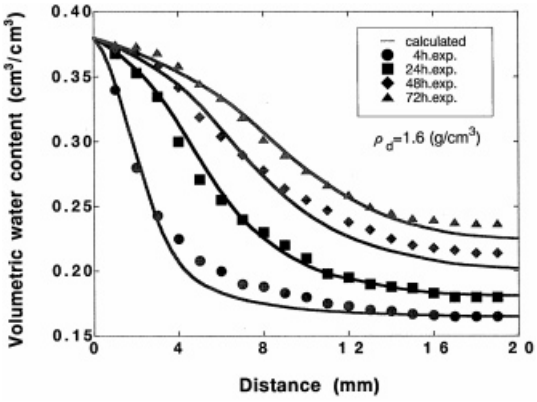


Figure 9. Distributions of volumetric water content

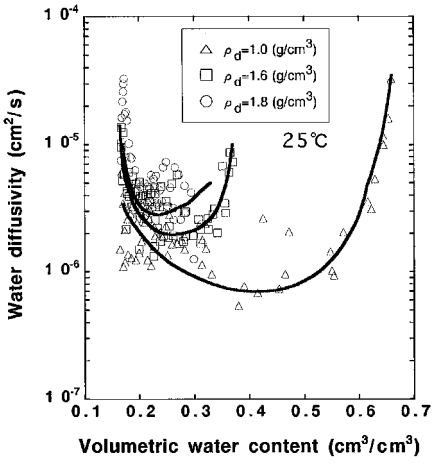


Figure 10. Dry density dependence of water diffusivity

yields

$$\frac{\partial \theta}{\partial t} = \frac{\partial}{\partial z}\left( D\,(\rho_{\mathrm{d}},\, T)\,\frac{\partial \theta}{\partial z}\right) \tag{9}$$

where $\rho_{\mathrm{d}}$ is the dry density. Then the distribution of the VWC is calculated from equation (9). The calculated result for the case of the dry density 1.6 g/cm$^3$ is expressed by solid lines in Figure 9. The calculated one precisely reproduced experimental one. The results of the other conditions also show the same tendency as this case. Thus, the validity of the determined water diffusivity was confirmed.

 

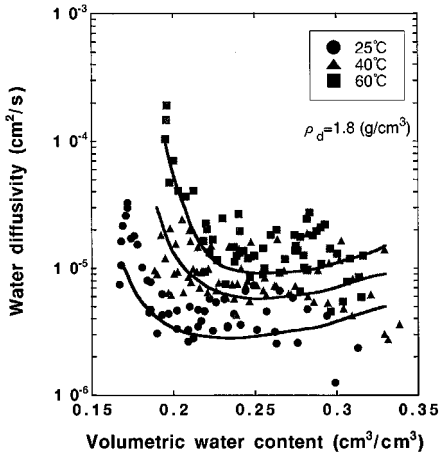


Figure 11. Temperature dependence of water diffusivity

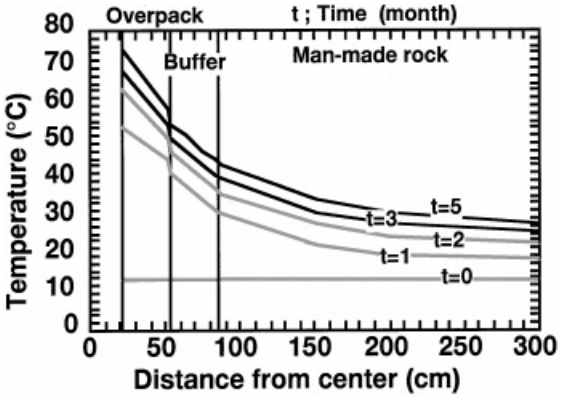


Figure 12. Time-dependent variation of temperature distribution

*The BIG-BEN test*

The variation of temperature distribution with time in the simulated overpack, buffer material and man-made rock in the horizontal plane through the heater centre at one of the vertical cross sections is shown in Figure 12. The contours of temperature (in °C) in a vertical cross section after 5 months are shown in Figure 13. Temperatures in the overpack and buffer material increased rapidly in the first month, then increased solwly thereafter. The temperature in the overpack on the heater side was approximately 75°C and approximately 60°C on the buffer material side. The maximum temperature of the bufer material was 55°C on the side of overpack and the minimum temperature was 46°C on the man-made rock side. The contours of water content (in %)

 

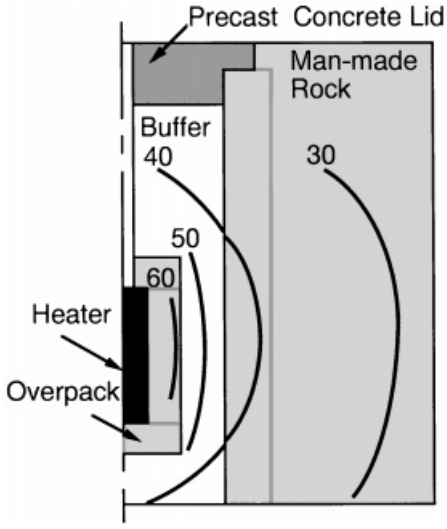


Figure 13. Contours of temperature after 5 months

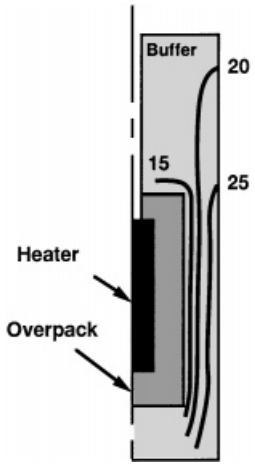


Figure 14. Contours of water content after 5 months

within the buffer material in a vertical cross-section after 5 months are shown in Figure 14. With time, the water content decreased on the overpack side, while it increased on the rock side. Figure 15 shows the variation of swelling pressure with time at different depths below the ground surface. The maximum swelling pressure obtained was about 0·4 MPa at the depth of the heater centre. The swelling pressures at other positions were lower than the maximum value. The reason that the swelling pressures for positions (1) and (6) exhibit peaks seems to be breakdowns of the sensors.

 

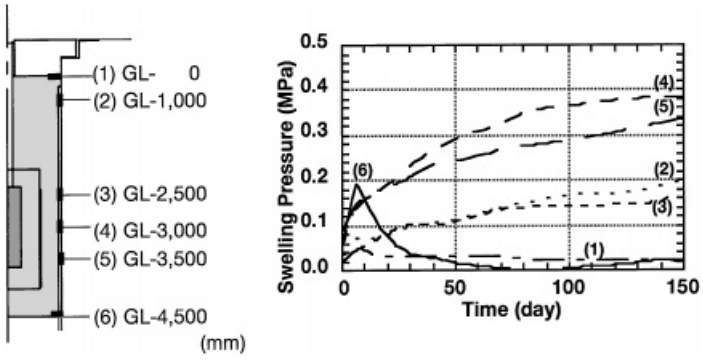


Figure 15. Time-dependent variation of swelling pressure

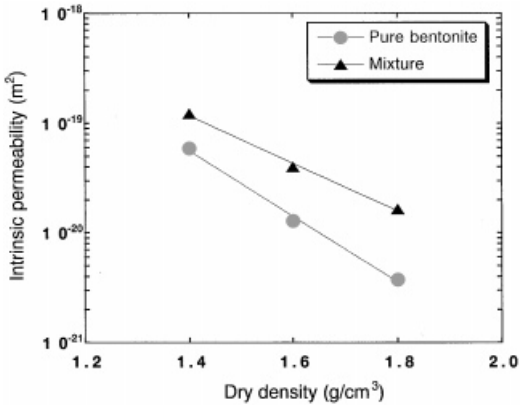


Figure 16. Dry density dependence of intrinsic permeability

## MODELLING OF WATER MOVEMENT IN SATURATED/UNSATURATED STATE

*Intrinsic permeability*

The measured intrinsic permeability of the pure benotnite specimen shows some scatter in the cases of higher dry densities, while other results show no temperature dependence. Thus, the scatter is thought to be measurement errors due to the limited amounts of the effluent (Figure 6).

Consequently, the temperature dependence of the hydraulic conductivity of the compacted bentonite is not due to the changes of properties of the solid matrix but is due to the changes of density and viscosity of the pore water.

The intrinsic permeability decreases with the increase in dry dentity, which is expressed by the following empirical formulae for the relationship between the dry density $\rho_d$ (g/cm$^3$) and the

 

intrinsic permeability $\kappa$ ($m^2$) (Figure 16):

$$\kappa = 8{\cdot}76 \times 10^{-16} \exp(-6.89\ \rho_d) \quad \text{(for the pure bentonite sample)}$$

$$\kappa = 1{\cdot}29 \times 10^{-16} \exp(-5.00\ \rho_d) \quad \text{(for the mixture sample)} \tag{10}$$

*Two-phase flow under isothermal condition*

As shown in Figures 10 and 11, the water diffusivity depends on dry density and temperature. The effects of the dry density and temperature on water diffusivity of bentonite are examined by separating the contributions of the vapour and liquid phases to the measured water diffusivity, and applying the Philip and de Vries' equation[8] to water vapour diffusivity and Darchy's equation to liquid water diffusivity. The Phillip and de Vries' equation under isothermal condition is expressed as

$$D_v = a\tau D_a v\rho^*\ h_r g\ \frac{1}{\rho_l}\frac{M}{RT}\frac{\partial\varphi}{\partial\theta} \tag{11}$$

and the Darcy's equation is expressed as

$$D_l = k\ \frac{\partial\varphi}{\partial\theta} \tag{12}$$

where $D_v$ is the water vapour diffusivity under isothermal condition, $a$ is the air-filled porosity, $\tau$ is the tortuosity allowing for the extra path length, $D_a$ is the diffusion coefficient for water vapour in air, $v$ is the mass flow factor, $\rho^*$ is the density of saturated water vapour, $h_r$ is the relative humidity $P/P_0$, $D_1$ is the liquid water diffusivity, and $k$ is the unsaturated hydraulic conductivity for the liquid phase. The mass flow factor is calculated from

$$v = P_T/(P_T - P) \tag{13}$$

where $P_T$ is the total gas pressure. Values of the diffusion coefficient for water vapour $D_a$ in $cm^2/s$ and the density of saturated water vapour are given in the literature.[8,16] The relative humidity is obtained by the psychrometric measurements. Values of other parameters are estimated as follows:

*1. Dry density dependence.* To identify the controlling factor in the dry density dependence of water diffusivity, the dry density dependence of each factor of the theoretical equations is examined. In the examination, water diffusivity is divided into water vapour and liquid water diffusivities. Equation (11) is applied to the water vapour diffusivity and equation (12) to the liquid water diffusivity. For estimating the liquid water diffusivity, it is assumed as a first approximation that the vapour and liquid phases contribute equally to the minimum value of the observed water diffusivity in the U-shaped curve for simplicity. Then the liquid water diffusivity ($D1$(est.)) is estimated by connecting this point and the observed water diffusivity ($D$(exp.)) at saturation point with a smooth curve. On the other hand, the water vapour diffusivity ($D$v(est.)) is calculated by subtracting the liquid water diffusivity ($D1$(est.) from the obtained water diffusivity ($D$(exp.)) (Figure 17).

In equation (11), the term $ah_r$ decreases with the increase in the dry density (Figure 18). Since the calculated tortuosities ($\tau$), almost in the range of 0·01–1, show no clear dry density dependence

 

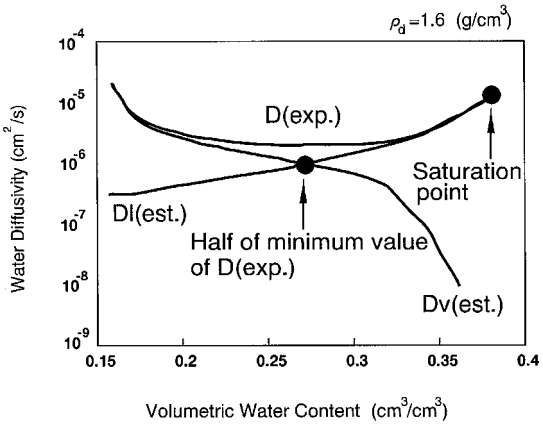


Figure 17. Separation of measured water diffusivity

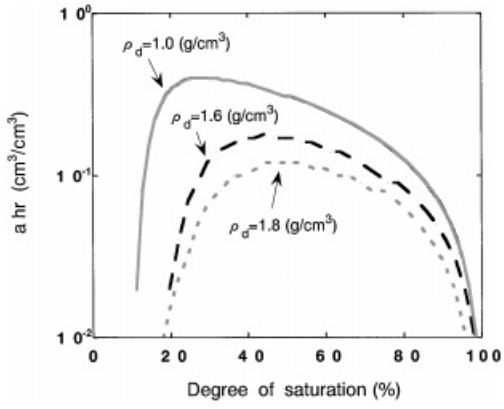


Figure 18. Dry density dependence of "a hr"

(Figure 19), the term $\tau D_a v \rho^* M/(RT)$ does not vary with the dry density. The term $\partial\varphi/\partial\theta$ increases with the dry density (Figure 20). Therefore the dry density dependence of the water vapour diffusivity is found to be mainly controlled by the potential gradient, $\partial\varphi/\partial\theta$.

In equation (12), the unsaturated hydraulic conductivity decreases with the increase of the dry density (Figure 21), while the potential gradient, $\partial\varphi/\partial\theta$ increases with the increase of the dry density. Therefore the liquid water diffiusivity is found to be also controlled by the potential gradient, $\partial\varphi/\partial\theta$.

*2. Temperature dependence.* The observed temperature dependence of the water diffusivity is compared with calculated results with equations (11) and (12). The water diffusivity at the temperatures of 40 and 60°C are calculated based on the tortuosity and unsaturated hydraulic conductivity at the temperature of 25°C. In this case, it is hypothesized that (1) the tortuosity is

 

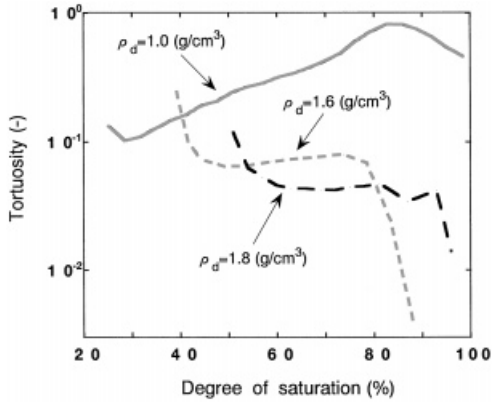


Figure 19. Dry density dependence of tortuosity

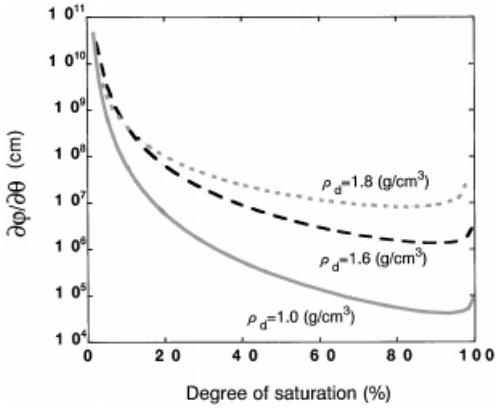


Figure 20. Dry density dependence of water potential gradient

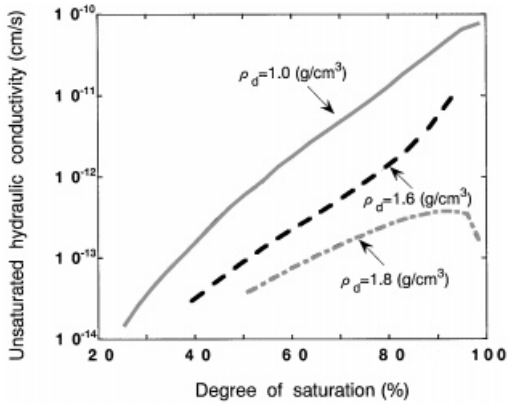


Figure 21. Dry density dependence of unsaturated hydraulic conductivity

 

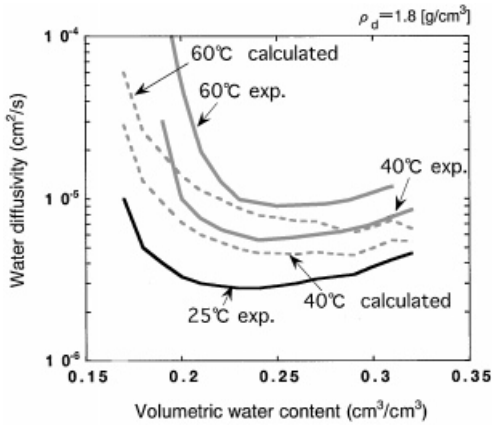


Figure 22. Comparison of measured and calculated water duffusivities

indepenent of the temperature, (2) the temperature dependence of the unsaturated hydraulic conductivity is attributed to the temperature dependence of the density and viscosity of water according to the intrinsic permeability concept applied to the saturated conductivity. The calculated results show good agreement with the experimental ones (Figure 22). Thus, the temperature dependence of the water diffusivity can also be explained by the Phillip and de Vries' equation and Darcy's equation.

## NUMERICAL ANALYSIS FOR BIG-BEN TEST

### *Theory of analysis*

Ohnishi *et al.*[17] have developed a FEM code THAMES to analyse the coupled T-H-M phenomena in a non-expansive saturated–unsaturated porous medium. However, this code could not treat the evaporation behaviour. In order to analyse the results of the BIG-BEN test, the code is modified to take vapour movement and swelling behaviour into account. The equation of water flow used in the modified THAMES code is based on the equation by Phillip and de Vries[8] and the findings from the laboratory experiments described above.

*1. Water flow model.* The equation of continuity for water, which takes into account the compressibility of the solid and density change by heat transfer is given by Ohnishi *et al.*:[17]

$$\{\rho_l k(\theta)(\psi + z)_{,i}\}_{,i} = -\rho_{l0} n \mathrm{Sr} \beta_T \frac{\partial T}{\partial t}$$

$$+ \rho_{l0} n \mathrm{Sr} \rho_l g \beta_P \frac{\partial h}{\partial t} + \rho_l \mathrm{Sr} \frac{\partial u_{i,i}}{\partial t} + \rho_l C(\psi) \frac{\partial \psi}{\partial t} \tag{14}$$

where $h$ is the total head expressed as the sum of the pressure head $\psi$ and the elevation head $z$, $n$ is the porosity, Sr is the degree of saturation, $\beta_P$ is the compressibility of water, $\beta_T$ is the thermal

 

expansion coefficient of water, $C(\psi)$ is the specific water capacity defined as $\partial\theta/\partial\psi$, $u_i$ is the displacement vector, $T$ is temperature, and $t$ is time. The subscript, 0, denotes the reference state. The term on the left-hand side represents the negative value of the gradient of mass flux, the first and second terms on the right-hand side mean the density change of pore water due to temperature change and due to total head, respectively, the third term means the change in volume of the porous medium matrix, and the fourth term means the change in water storage capacity. In the mass flux term of equation (14), the water vapour movement and heat-induced water movement are not taken into account. The mass flux $q$ including those components of the water movements is expressed as[8]

$$q = -\rho_1 D_v \nabla\theta - \rho_1 D_l \nabla\theta - \rho_1 k \nabla z - \rho_1 D_T \nabla T \tag{15}$$

where $D_T$ is the thermal water diffusivity. The terms on the right-hand side are rewritten using the intrinsic permeability concept, equation (2), expressions shown in equations (5) and (12), and the fact that the osmotic potential is negligible in the case of bentonite,

$$q = -\rho_1 D_v \frac{\partial\theta}{\partial\varphi} \nabla\varphi - \rho_1 \frac{\rho_1 g \kappa K_r}{\mu} \nabla(\varphi + z) - \rho_1 D_T \nabla T \tag{16}$$

where $K_r$ is the relative permeability which is the ratio of the unsaturated permeability to the saturated permeability. Taking the matric potential as the pressure head ($\varphi = \psi$) and substituting equation (16) for the mass flux in equation (14), the equation of continuity for water is obtained as

$$\left\{\rho_1 D_v \frac{\partial\theta}{\partial\psi} \psi_{,i} + \frac{\rho_1^2 g \kappa K_r}{\mu} h_{,i}\right\}_{,i} + \{\rho_1 D_T T_{,i}\}_{,i}$$

$$- \rho_{10} n \mathrm{Sr}\, \rho_1 g \beta_P \frac{\partial h}{\partial t} - \rho_1 C(\psi) \frac{\partial h}{\partial t} - \rho_1 \mathrm{Sr} \frac{\partial u_{i,i}}{\partial t} + \rho_{10} n \mathrm{Sr} \beta_T \frac{\partial T}{\partial t} = 0 \tag{17}$$

*2. Heat transfer model.* The equation of energy conservation, in which stress-deformation and groundwater flow are considered, is also given by Ohnishi *et al.*:[17]

$$(\rho C_v)_m \frac{\partial T}{\partial t} + n \mathrm{Sr} \rho_f C_{vf} V_f \cdot \nabla T$$

$$= \nabla \cdot K_{Tm} \nabla T - n \mathrm{Sr} T \frac{\beta_T}{\beta_P} k(\theta) h_{,ii} \tag{18}$$

$$- \frac{1}{2}(1 - n) \beta T \frac{\partial}{\partial t}(u_{i,j} + u_{j,i}) \delta_{ij}$$

in which

$$\beta = (3\lambda_l + 2\mu_l)\alpha \tag{19}$$

where $(\rho C_v)_m$ is the specific heat capacity of the field consisting of water and the structured particles, $\rho_f$ is the density of the fluid, $C_{vf}$ is the heat capacity of the fluid, $V_f$ is the velocity of the fluid, $K_{Tm}$ is the thermal conductivity of the field, $\delta_{ij}$ is Kronecker's delta, $\lambda_l$ and $\mu_l$ are Lame's constants, and $\alpha$ is coefficient of linear expansion. The first term on the left-hand side of equation (18) shows the time dependence of energy, and the second term shows the energy change due to heat convection. The first, second and third terms on the right-hand side express the energy change due to heat conduction, pore pressure change and reversible energy change caused by

 

solid deformation, respectively. Since the water flux in equation (18) takes only that in the liquid phase into account, the same expansion used in the water flow model (equation (16)) can be applied. The second term on the left-hand side may be expressed to take into account the heat conduction by both liquid and vapour phases as

$$n\mathrm{Sr}\rho_{\mathrm{f}}\ C_{\mathrm{vf}}V_{\mathrm{f}}\nabla T = \theta_{\mathrm{l}}\rho_{\mathrm{l}}C_{\mathrm{vl}}V_{\mathrm{l}}\nabla T + \theta_{\mathrm{v}}\rho_{\mathrm{v}}C_{\mathrm{vv}}V_{\mathrm{v}}\nabla T \tag{20}$$

where $\theta_{\mathrm{l}}$ is the volumetric liquid water content, $C_{\mathrm{vl}}$ is the heat capacity of liquid water, $V_1$ is the velocity of liquid water, $\theta_{\mathrm{v}}$ is the volumetric water vapour content, $\rho_{\mathrm{v}}$ is the density of water vapour, $C_{\mathrm{vv}}$ is the heat capacity of water vapour and $V_{\mathrm{v}}$ is the velocity of water vapour. However, the second term on the right-hand side of equation (20) is omitted for simplicity at the stage of this study. The second term on the right-hand side of equation (18) is expressed as

$$-\,n\ \mathrm{Sr}T\,\frac{\beta_{\mathrm{T}}}{\beta_{\mathrm{P}}}\left\{D_{\mathrm{v}}\,\frac{\partial\theta}{\partial\psi}\,\psi_{,i} + \frac{\rho_{\mathrm{l}}g\kappa K_{\mathrm{r}}}{\mu}\,h_{,i} + D_{\mathrm{T}}T_{,i}\right\}_{,i}$$

Furthermore, the latent heat transfer should be added to the heat transmission mechanisms. The heat conduction equation including the latent heat transfer is given by Phillip and de Vries[8] as

$$(\rho C_{\mathrm{v}})_m\,\frac{\partial T}{\partial t} = \nabla\cdot(K_{\mathrm{T}m}\,\nabla T) - L\nabla\cdot(D_{\mathrm{v}}\,\nabla\theta) \tag{21}$$

where $L$ is the latent heat of vapourization of unit volume of water. The term for the latent heat transfer can be rewritten as

$$-\,L\nabla\,(D_{\mathrm{v}}\nabla\theta) = -\,L\,\left\{D_{\mathrm{v}}\,\frac{\partial\theta}{\partial\psi}\,(h_{,i} - z_{,i})\right\}_{,i} \tag{22}$$

Thus, the modified equation for the heat transfer is given as

$$\begin{aligned}(\rho C_{\mathrm{v}})_m\,\frac{\partial T}{\partial t} + n\mathrm{Sr}\rho_{\mathrm{l}}C_{\mathrm{vl}}V_{\mathrm{l}}T_{,i} - K_{\mathrm{T}m}T_{,ii} + L\left\{D_{\mathrm{v}}\,\frac{\partial\theta}{\partial\psi}\,(h_{,i} - z_{,i})\right\}_{,i}\\ + n\mathrm{Sr}T\,\frac{\beta_{\mathrm{T}}}{\beta_{\mathrm{P}}}\left\{D_{\mathrm{v}}\,\frac{\partial\theta}{\partial\psi}\,(h_{,i} - z_{,i}) + \frac{\rho_{\mathrm{l}}g\kappa K_{\mathrm{r}}}{\mu}\,h_{,i} + D_{\mathrm{T}}T_{,i}\right\}_{,i}\\ + \frac{1}{2}\,(1-n)\,\beta T\,\frac{\partial}{\partial t}\,(u_{i,j} + u_{j,i})\,\delta_{ij} = 0\end{aligned} \tag{23}$$

*3. Mechanical model.* For an isotropic linear elastic material, the equilibriuim equation which takes into account the effects of heat transfer and pore pressure change is given[17] by

$$\left\{\frac{1}{2}\,C_{ijkl}\,(u_{k,\mathrm{l}} + u_{\mathrm{l},k}) - \beta\delta_{ij}\,(T - T_0) + \chi\delta_{ij}\,\rho_{\mathrm{f}}\,g\psi\right\}_{,\,j} + \rho b_i = 0 \tag{24}$$

where $C_{ijkl}$ is the elastic matrix, $\rho$ is the density of the medium and $b_i$ is the body force. $\chi$ is the parameter proposed by Bishop and Blight[18] for the effective stress principle for a saturated–unsaturated medium as

$$\begin{aligned}\sigma_{ij} &= \sigma'_{ij} + \chi\ \delta_{ij}\rho_{\mathrm{f}}g\psi,\\ \chi &= \begin{cases} 1 & \text{saturated}\\ \chi(\mathrm{Sr}) & \text{unsaturated}\end{cases}\end{aligned} \tag{25}$$

where $\sigma_{ij}$ is the total stress and $\sigma$'$_{ij}$ is the effective stress.

 

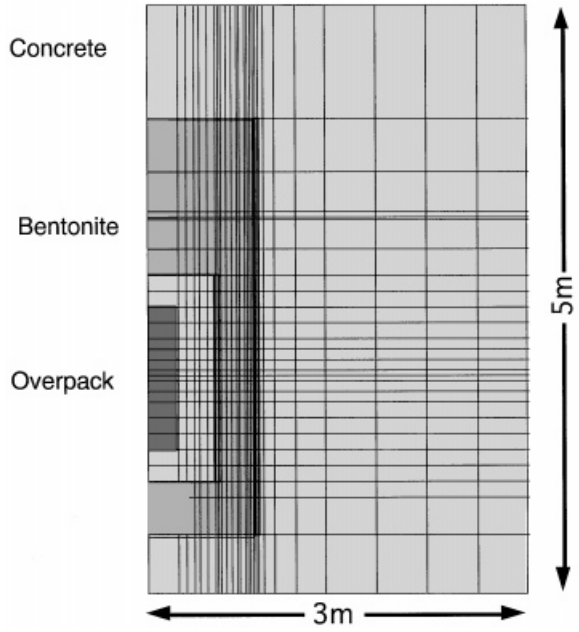


Figure 23. Mesh used in the FEM analysis

In this study, $\chi$ is assumed to be equal to the degree of saturation and the equilibrium equation is modified to take the swelling behaviour into account as

$$\left\{\frac{1}{2} C_{ijkl} (u_{k,l} + u_{l,k}) - \pi\delta_{ij} - \beta\delta_{ij} (T - T_0) + \chi\delta_{ij}\rho_f g\psi\right\}_{,j} + \rho b_i = 0 \tag{26}$$

where $\pi$ is the swelling pressure. The swelling pressure is assumed, as a first approximation, to be

$$\pi = v\Delta\theta \tag{27}$$

where $v$ is a coefficient relating to the swelling pressure process.

*Finite element formulation and calculation method*

The method used for the finite element discretization is the Galerkin-type formulation. The linear quadrilateral isoparametric element for $h$ and $T$, and the quadratic quadrilateral element for $u_i$ are employed in the code. In order to integrate time derivatives, an accelerator was introduced.[17]

Figure 23 shows the mesh used in the FEM analysis. The calculation is carried out as an axisymmetric problem. The numbers of nodes and elements used in the calculation are 2533 and 806, resepectively. The initial and boundary conditions are summarized in Table IV. Heat is assumed to be generated uniformly from the exothermic part which is composed of glass beads.

 

Table IV. Initial and boundary conditions for the analysis of BIG-BEN test

| Item | Property | Value/condition |
|---|---|---|
| Initial condition | Temperature (°C) | 1·5 |
| | Water content (%) | 16·5 |
| | Void ratio ( − ) | 0·69 |
| | Effective mean stress (MPa) | 0·02 (radial)<br>0·05 (vertical) |
| | Pore water pressure (MPa) | − 14·3 |
| Boundary condition | Thermal | Heat transfer coefficient<br>1.16 (W/m$^2$ K) |
| | Hydraulic | Fixed 0·05 (MPa) |
| | Mechanical | Slider |

Water injection is defined with fixed pressure of 0.05 MPa at nodal points which is equal to water injection slot.

*Parameters*

Parameters of man-made rock, glass beads, simulated overpack and the buffer material used in this analysis are compiled in Table V.[19] The properties of the man-made rock, glass beads and overpack were collected by literature surveys. The various properties of liquid water and water vapor are given in the literature.[8,16] The properties of the buffer material were determined based on laboratory measurements. The thermal conductivity $K_{Tm}$ (W/mK), specific heat $(\rho C_v)_m$ (kJ/m$^3$ $K$), suction $|\varphi|$ (cm) and thermal water diffusivity $D_T$ (cm$^2$/sK) of the buffer material are given in the following equations:

$$K_{Tm} = 0{\cdot}33 + 0{\cdot}031\theta \tag{28}$$

$$(\rho C_v)_m = (100 + 4{\cdot}2w)/(100 + w) \tag{29}$$

$$|\varphi| = (1{\cdot}06 \times 10^6) \times 10^{-0.0325\theta} \quad (\text{at } T = 25^\circ\text{C})$$

$$|\varphi| = (8{\cdot}81 \times 10^5) \times 10^{-0.0334\theta} \quad (\text{at } T = 50^\circ\text{C}) \tag{30}$$

$$D_T = 9{\cdot}0 \times 10^{-10} \exp\left(1{\cdot}8 \times \frac{T - 25}{25}\right) \tag{31}$$

where $w$ is the water content and $T$ is the temperature in °C. In this analysis, the isothermal water flux terms, shown in the first and second terms on the right-hand side of the equation (16), are not handled separately but handled with the isothermal water diffiusivity. Therefore, parameters for the intrinsic permeability and relative permeability of the buffer material are not used explictly. The isothermal water diffusivity for the specimen used in the BIG-BEN test is shown in Figure 24.[19]

 

Table V. Parameters for the analysis of BIG-BEN test

| Material | Property | Value |
|---|---|---|
| Man-made rock | Density (g/cm$^3$) | 2·3 |
| | Young's modulus (MPa) | $2{\cdot}5 \times 10^4$ |
| | Poisson's ratio ( − ) | 0·167 |
| | Thermal conductivity (W/mK) | 1·88 |
| | Specific heat (kJ/kgK) | 0·75 |
| | Coefficient of linear expansion (1/K) | $1{\cdot}00 \times 10^{-5}$ |
| Glass beads | Density (g/cm$^3$) | 1·6 |
| | Young's modulus (MPa) | $8{\cdot}2 \times 10^4$ |
| | Poisson's ratio ( − ) | 0·3 |
| | Thermal conductivity (W/mK) | 0·255 |
| | Specific heat (kJ/kgK) | 0·84 |
| | Coefficient of linear expansion (1/K) | $1{\cdot}00 \times 10^{-5}$ |
| Overpack | Density (g/cm$^3$) | 7·8 |
| | Young's modulus (MPa) | $2{\cdot}0 \times 10^5$ |
| | Poisson's ratio ( − ) | 0·3 |
| | Thermal conductivity (W/mK) | 53·0 |
| | Specific heat (kJ/kgK) | 0·46 |
| | Coefficient of linear expansion (1/K) | $1{\cdot}64 \times 10^{-5}$ |
| Buffer material | Initial dry density (g/cm$^3$) | 1·6 |
| | Initial water content (%) | $16{\cdot}5 \pm 1{\cdot}0$ |
| | Young's modulus (MPa) | 27 ($w = 16{\cdot}8$) |
| | | 10 ($w = 25{\cdot}9$) |
| | Poission's ratio ( − ) | 0·4 |
| | Saturated hydraulic conductivity (m/s) | $4{\cdot}0 \times 10^{-13}$ |
| | Coefficient of linear expansion (1/K) | $1{\cdot}0 \times 10^{-4}$ |
| | Coefficient for the swelling process $v$(MPa) | 1·7 |
| | Thermal conductivity (W/mK) | equation (28) |
| | Specific heat (kJ/m$^3$ K) | equation (29) |
| | Suction (cm) | equation (30) |
| | Isothermal water diffusivity (cm$^2$/2) | Figure 24 |
| | Thermal water diffusivity (cm$^2$/sK) | equation (31) |

*Results of analysis*

Figure 25 shows the comparison of measured temperatures with the calculated ones. The calculated results of temperature in the buffer material are approximately 5 degrees lower than those of the measured results. The reason of this difference may be due to inappropriateness of the heat transfer boundary condition used in the calculation. However, the calculated results of the distributions or gradients of the temperature are in fair agreement with the measured results. Figure 26 shows the comparison of water content. The calculated results of the water content also fairly reproduce the measured distributions of the water content, which are affected by the temperature gradient. The water contents of both measured and calculated results increase to 25% on the rock side and decrease below 15% on the overpack side at the level of GL–3·0 m. Figure 27 shows calculated results of horizontal stress distributions after 5 months. The calculated stresses are considerably lower than the swelling pressure measured in the test.

 

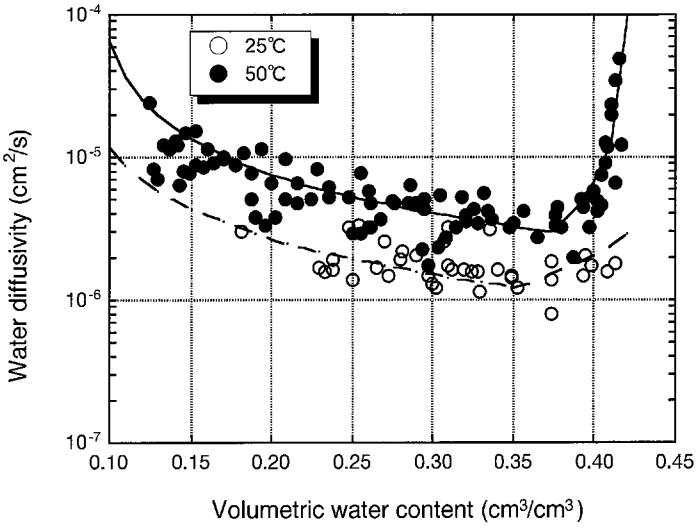


Figure 24. Isothermal water diffusivities of the specimen for BIG-BEN test

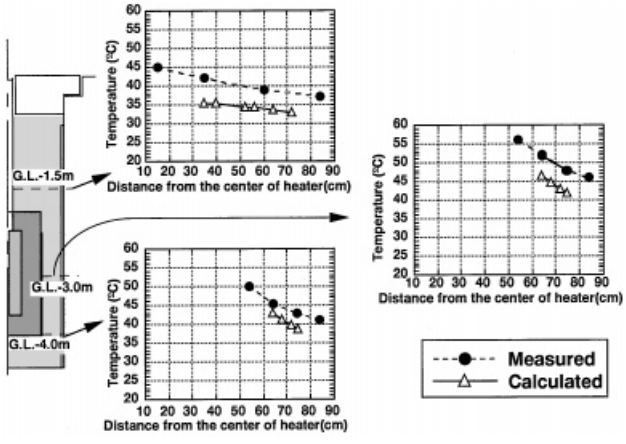


Figure 25. Temperature distributions with radial distance after 5 months

Thus, stress changes due to the swelling of the buffer material could not be properly quantified by this numerical analysis, while the heat transfer and water movement under thermal gradient could be fairly predicted. As to the mechanical behaviour of the bentonite buffer, the model for the swelling process used in this analysis is still phenomenological. Further investigations to obtain a framework for the modelling including the mechanism of the process are required.

 

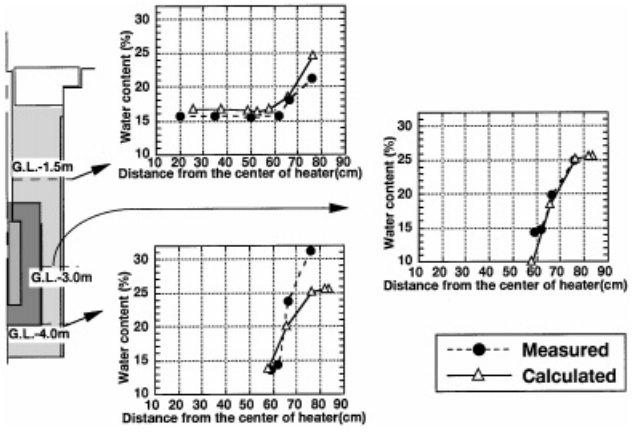


Figure 26. Water content distributions with radial distance after 5 months

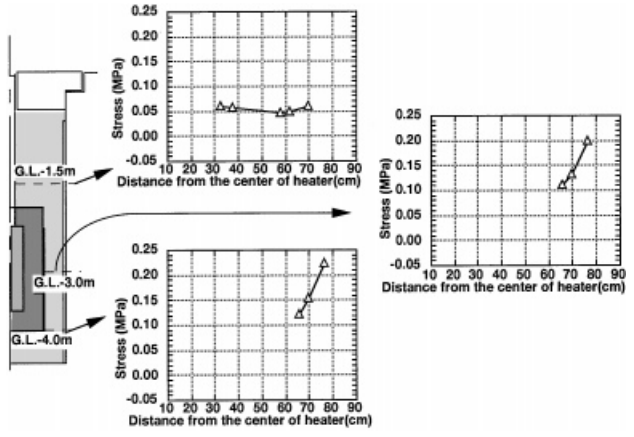


Figure 27. Calculated results of vertical stress distributions with radial distance after 5 months

## CONCLUDING REMARKS

Mechanistic models of water movements in both saturated and unsaturated states for the bentonite buffer material have been developed based on the small-scale laboratory experiments. The temperature dependence of the saturated hydraulic conductivity of bentonite-based buffer material is examined by the intrinsic permeability concept and the dependence is concluded to be due to changes in the viscosity and density of pore water. For the water movement in unsaturated state, the application of Philip and de Vries' equation and Darcy's equation can explain the dry density and temperature dependence of the water diffusivity for compacted bentonite.

 

Results of the full-scale T-H-M test on the engineered barrier including the bentonite buffer material and numerical analysis for the test based on the current knowledge of the coupled T-H-M processes in compacted bentonite are presented. The calculated results have fairly reproduced the test results except for mechanical phenomena.

Since coupled T-H-M analysis for the bentonite buffer is essential for a safety assessment of the geological disposal, efforts at mechanism clarification, parameter identification, and physical and mathematical model development should be continued. PNC has planned a full-scale *in situ* experiment[20] on the coupled T-H-M process for the buffer material and surrounding rock at the Kamaishi mine is Japan to develop a fully coupled T-H-M model.

## ACKNOWLEDGEMENTS

The authors are grateful to Associate Professor A. Kobayashi of Iwate University and Dr. K. Amemiya and Mr. M. Chijimatsu of Hazama Corporation for providing valuable comments and suggestions and to Messrs. H. Suzuki and K. Matsumoto of Inspection Development Corporation for their excellent technical assistance.

## REFERENCE

1. Power Reactor and Nuclear Fuel Corporation, 'Research and development on geological disposal of high-level radioactive waste. First progress report', *PNC TN1410 93-012*, 1992.
2. R. Pusch, 'Permeability of highly compacted bentonite', *KBS Technical Report*, *TR 80-16*, 1980.
3. H. S. Radhakrishna and H. T. Chan, 'Strength and hydraulic conductivity of clay-based buffers for a deep underground nuclear fuel waste disposal vault', Atomic Energy of Canada Ltd., *Tech. Rec.*, *TR-327*, 1985.
4. Nagra (National Cooperative for the Storage of Radioactive Waste), *Nagra Project Report*, NGB85-09, 1985.
5. J. Bear, *Hydraulics of Groundwater*, McGraw-Hill, New York, 1979, pp. 66–67.
6. L. Börgesson, 'Water flow and swelling pressure in non-saturated bentonite clay barriers', *Engng Geol.*, **21,** 229–237 (1985).
7. T. Kanno and H. Wakamatsu, 'Water uptake and swelling properties of unsaturated bentonite buffer materials', *Can. Geotech. J.*, **29,** 6 (1992).
8. J. R. Philip and D. A. de Vries, 'Moisture movement in porous materials under temperature gradients', *Am. Geophys. Union Trans*, **38**(2) (1957).
9. M. Nakano, Y. Amemiya and K. Fujii, 'Saturated and unsaturated hydraulic conductivity of swelling clays', *Soil Sci.*, **141,** 1–6 (1986).
10. S. Sato, A. Kobayashi, K. Hara, H. Ishikawa and N. Sasaki, 'Full scale test on coupled thermo-hydro-mechanical process in engineered barrier system', *Proc. '91 Joint Int. Waste Management Conf.*, ASME, Seoul, Korea, 1991.
11. K. Smith and C. Mullins, *Soli Analysis — Physical Methods*, Marcel Dekker, New York, 1991.
12. M. Nakano, Y. Amemiya, K. Fujii, T. Ishida and Y. Ishii, 'Infiltration and volumetric expansion in unsaturated clay', *Trans. Jpn. Soc. Irrig. Reclam.*, **100,** 8–16 (1982) (in Japanese).
13. H. Ishikawa, K. Amemiya, Y. Yusa and N. Sasaki, 'Comparison of fundamental properties of Japanese bentonite as buffer material for waste disposal', *Proc. 9th Int. Clay Conf.*, Strasbourg, France, 1989.
14. M. Th. van Genuchten, 'A closed-form equation for predicting the hydraulic conductivity of unsaturated soils', *Soli Sci. Soc. Am. J.* **44,** 892–898, (1980).
15. Power Reactor and Nuclear Fuel Corporation, 'Finite element non-linear structural analysis system FINAS, Version 11.0' *PNC N9520 89-019*, 1989 (in Japanese).
16. National Astronomical Observatory, *Rika nenpyo* (*Chronological Scientific Tables*, Maruzen Co., Ltd., 1990 (in Japanese).
17. Y. Ohnishi, H. Shibata and A. Kobayashi, 'Development of finite element code for the analysis of coupled thermo-hydro-mechanical behaviors of a saturated-unsaturated medium', in *Coupled Processes Associated with Nuclear Waste Repositories*, Academic Press, New York, 1989, pp. 679–697.
18. A. W. Bishop and G. E. Blight, 'Some aspects of effective stress in saturated and partly saturated soil', *Geotechnique*, **13** (3)**,** (1963)

 

19. T. Fujita, A. Kobayashi and L. Börgesson, 'Experimental investigation and mathematical simulation of coupled T-H-M processes of the engineered buffer materials (TC3)', in C.F. Tsang, O. Stephansson and J. L. Jing (eds), *Mathematical Modelling and Experimental Studies of Coupled Thermo-Hydro-Mechanical Processes in Fractured Media.—Recent Development Based on the DECOVALEX-Project on Issues Related to Geological Disposal of Radioactive Waste*, Chapter 14, Elsevier Publisher, Amsterdam, 1997.
20. T. Fujita, Y. Sugita, H. Ishikawa and T. Mano, 'Plan of coupled thermo-hydro-mechanical experiment at the Kamaishi mine', *PNC TN8020 94-005*, 1995.

 